

Storm wave clustering around New Zealand and its connection to climatic patterns

Victor A. Godoi,^{a*}  Karin R. Bryan^a and Richard M. Gorman^b

^a School of Science, University of Waikato, Hamilton, New Zealand

^b National Institute of Water and Atmospheric Research, Hamilton, New Zealand

ABSTRACT: Clusters of storm waves contribute disproportionately to coastal erosion hazards because the coastline has insufficient time to recover between events. Here, the change in occurrence of clustered storms and its association with atmospheric oscillation modes were investigated in New Zealand waters using 44 years (1958–2001) of wave hindcast data. First, long-term averages of cluster parameters (number of storms within the cluster, potential for coastal erosion, and cluster duration) were assessed. Then, the relationships between clustering and the El Niño-Southern Oscillation (ENSO), Indian Ocean Dipole (IOD), Zonal Wavenumber-3 Pattern (ZW3), Pacific Decadal Oscillation (PDO), and Southern Annular Mode (SAM) were explored through correlation analysis over several timescales. Clusters were more frequently observed to the northeast of New Zealand and on the central eastern coast of the South Island. The most vulnerable regions to cluster-induced coastal erosion were southern New Zealand and the northwestern coast, which resulted from steady southwesterly swells, although clusters with the longest duration occurred on the east coast of the South Island. Trends suggest that clusters have incorporated more storms, have become more hazardous, and have increased in duration, particularly along the South Island coastline. Although these trends may be sensitive to the reanalysed wind fields used to force the wave hindcast, they reflect trends in the ENSO, PDO, and SAM. Stronger southwesterly winds during El Niño (negative ENSO) and El Niño-like conditions (positive IOD/PDO) generated more clustered storms mainly on the southwestern coast of New Zealand, whereas increases in clustering were observed on the north coast during La Niña and La Niña-like conditions (stronger northeasterly winds). Higher occurrence of clustering was also evident on the west coast during the strong atmospheric zonal flow associated with negative ZW3. Lastly, strengthened westerlies related to positive SAM led to increased clustering primarily to the south of New Zealand.

KEY WORDS storm wave clustering; storm grouping; climate patterns; climate change; coastal hazard; New Zealand; wave hindcasting

Received 27 April 2017; Revised 13 November 2017; Accepted 15 November 2017

1. Introduction

A combination of swell and locally generated waves is frequently observed along open coastlines influenced by different meteorological systems (Harley *et al.*, 2010). Such coastlines are highly impacted by storm waves, which in turn are potentially more hazardous when arriving in clusters because the intervals between the events are not sufficiently long for the beach to recover (Lee *et al.*, 1998; Senechal *et al.*, 2017). When propagating in clusters, storms with relatively short return periods can cause damage equivalent to or greater than that from a single storm with far longer return period (Ferreira, 2005). Consequently, clustered storms may produce catastrophic events in populated coastal areas. Therefore, an improved knowledge of storm wave clusters (SWCs) and of the changes in the frequency and magnitude of these systems over time is needed to support coastal management.

From a meteorological point of view, a cluster is characterized by unstable atmospheric waves that

develop and move rapidly along the wake of a large low-pressure system (Mailier *et al.*, 2006). From an oceanographic–morphodynamic point of view, a storm cluster can be defined as two or more consecutive storms between which there is insufficient time for the beach to recover from erosion (Ferreira, 2006). Atmospheric serial storms have been shown to have devastating effects on the European economy (e.g. Mailier *et al.*, 2006; Pinto *et al.*, 2013; Pinto *et al.*, 2014). Past work has also associated cyclone clustering (Mailier *et al.*, 2006; Economou *et al.*, 2015) and clustering of flooding events (Villarini *et al.*, 2013) with climatic patterns, such as the North Atlantic Oscillation. However, SWCs have been explored less because of the lack of data. Therefore, both their nearshore and offshore characteristics are still poorly understood. Despite that, they have been shown to play a role in the evolution of a number of coastal features, such as cliffs (Nunes *et al.*, 2011), megarips (Loureiro *et al.*, 2012), dunes (Benavente *et al.*, 2013; Dissanayake *et al.*, 2015a, 2015b, 2015c), and shoreline cusps (Balouin *et al.*, 2013).

Several techniques to identify groups of cyclones have been implemented, such as a Bayesian approach (Fawcett and Walshaw, 2008), a running sum of daily cyclone counts

*Correspondence to: V. A. Godoi, School of Science, University of Waikato, Hillcrest Rd, Hamilton 3216, Waikato, New Zealand. E-mail: victorgodoir@gmail.com

(Pinto *et al.*, 2014), and the calculation of a dispersion statistic based on the Poisson process and cyclone counts (Mailier *et al.*, 2006; Kvamstø *et al.*, 2008; Vitolo *et al.*, 2009). Studying cyclone clusters, however, does not necessarily provide useful information on the formation of SWCs. Large waves might not be generated if cyclones change direction continuously along their tracks, because the generation of large waves depends on persistent strong unidirectional winds.

In the past, SWCs were evaluated by measuring the beach morphodynamic response to a sequence of storms. This has been performed mainly through either beach profile assessments (e.g. Lee *et al.*, 1998; Loureiro *et al.*, 2009; Coco *et al.*, 2014; Karunaratna *et al.*, 2014) or detailed numerical or empirical modelling of erosion (e.g. Voudoukas *et al.*, 2011; Splinter *et al.*, 2014; Disanayake *et al.*, 2015a, 2015b, 2015c), although other approaches have also been implemented, such as the analysis of ARGUS video imaging (Phillips *et al.*, 2015) and the use of the convolution model of Kriebel and Dean (1993), applied by Ferreira (2002). These techniques either require long records of consistently monitored beach profiles or are computationally expensive and time-consuming. Most of the studies quoted above used beach recovery periods (i.e. the average time interval the beach takes to recover substantially after an erosion) to identify SWCs. Beach erosion and recovery are not trivial to ascertain because they require surveying before, during, and after each storm within the cluster. The local intensity of the storm, the beach state, the tide conditions, and the type and availability of sediment have a strong influence on variability of the beach recovery period, making it highly site-dependent. Furthermore, slightly different combinations of these parameters can lead to significantly different erosion and recovery responses, especially when the initial stage has already been disturbed (Coco *et al.*, 2014). For these reasons, SWCs have been analysed only at a particular beach or, at most, at several beaches. Considerable variation exists in the time thresholds that determine which storms belong to a single cluster. For example, Birkemeier *et al.* (1999) grouped storms that occurred up to 40 days apart at Duck, United States. Ferreira (2005) stated that either 21 days between storm peaks or 14 days between the end of a storm and the beginning of the subsequent one was enough to ensure that beaches would not recover significantly at his study sites, in Portugal. Karunaratna *et al.* (2014) considered a 9-day cut-off to define clustered storms at Narrabeen Beach, Australia, whereas Almeida *et al.* (2012) aggregated storms that occurred less than 10 days apart on the Portuguese coast.

Located at the interface between the Pacific and Southern Oceans, with the Tasman Sea to the west, patterns of storm clustering around New Zealand are likely to be complex, depending on the origin of generating weather systems. As an island nation, New Zealand is reliant on shipping for trading goods. Moreover, the implementation of recent trade agreements (summarized in, e.g. World Bank Group, 2016) has led to increased ship traffic, and the energetic seas surrounding New Zealand (Gorman

et al., 2003) mean that assessing conditions and providing predictions for maritime safety has become increasingly important. New Zealand's mid-latitude position and distance from other landmasses allow several weather systems to affect the country, causing frequent storms and extreme wave events (Godoi *et al.*, 2017). These wave conditions have been shown to vary considerably in association with climate patterns (Godoi *et al.*, 2016). Changes in the Southern Hemisphere atmospheric circulation related to the Southern Annular Mode (SAM) (Thompson and Solomon, 2002), such as a polewards shift of the westerly jet and associated fields (Kushner *et al.*, 2001), affect New Zealand directly. The SAM is the dominant mode of atmospheric variability in the Southern Hemisphere (Marshall, 2003) and is associated with the formation of extratropical cyclones, the main source of the storm waves that affect the New Zealand coastline. However, SWCs and their characteristics have not been investigated in the New Zealand region yet. The lack of high temporal resolution beach profiles and other data sets for most New Zealand beaches limits the ability to study clustering through erosion responses. As a first step, we use our long-term (1957–2002) wave hindcast (Gorman *et al.*, 2010) to investigate the drivers of storm clustering.

Given the recognized threat posed by SWCs to coastal environments and infrastructure, as well as to offshore operations (e.g. oil rigs and fishery boats), this study explores the relationships of SWCs to climate patterns in New Zealand waters. A SWC climatology supports not only the monitoring and management of coastal areas in terms of flooding and sediment transport but also the planning of naval and marine operations, besides assisting in the selection of sites for wave energy extraction. Our investigation was carried out using the results of our long-term wave hindcast and considers how conditions might change in association with five climate patterns, as characterized by the El Niño-Southern Oscillation (ENSO), Indian Ocean Dipole (IOD), SAM, Pacific Decadal Oscillation (PDO), and Zonal Wavenumber-3 Pattern (ZW3). First, duration and number of clusters in addition to the potential for cluster-induced coastal erosion were assessed through average values computed over the period 1958–2001. To account for changes in the frequency and magnitude of SWC generating systems (cyclones) and those changes that have an indirect impact on them, like changes in atmospheric ozone and greenhouse gases (Arblaster and Meehl, 2006), monotonic trends in SWC parameters (cluster duration, number of storms within the cluster, and cumulative storm energy (CSE)) were calculated. Then, correlations of climate indices with clustered storms and SWC parameters were carried out at multiple timescales to better understand the causes of variability in clustering.

2. Methodology

A 45-year (September 1957 to August 2002) wave hindcast (Gorman *et al.*, 2010), hereafter 45WH, was conducted using version 3.14 (Tolman, 2009) of the

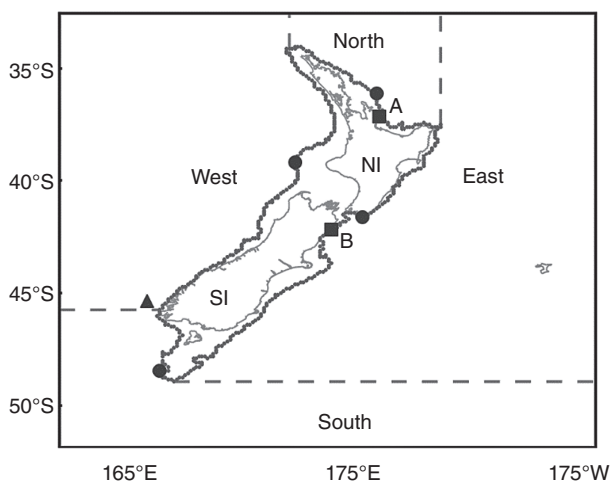


Figure 1. Regional domain of the 45-year (1957–2002) wave hindcast. Filled circles represent the locations used in the wavelet spectral analysis. Filled squares A and B indicate the sites used as examples for showing time series of occurrence of clustered storms in Figures 2(b) and (c), respectively. Grey dots illustrate the model grid points on the 200 m isobath, with the filled triangle marking the first point (0) of the sequence of Figure 2(a). Dashed lines represent coastline delimiters, plotted here as a guide for Figure 2(a). NI and SI stand for North Island and South Island, respectively.

WAVEWATCH III model (Tolman, 1991) forced with wind and ice fields from the ERA-40 reanalysis (Uppala *et al.*, 2005). A regional domain, with $0.125 \times 0.09375^\circ$ spatial resolution, was one-way nested within a global domain at $1.125 \times 1.125^\circ$ resolution. The regional domain encompassed the waters surrounding New Zealand, which include part of the Tasman Sea and parts of the Southern Ocean and southwestern Pacific Ocean (Figure 1). Results of the simulation were output at 1 and 3-h intervals for the regional and global domains, respectively, and then validated against satellite altimetry data from the TOPEX/Poseidon, ERS1 and ERS2 missions, and against buoy measurements from sites around New Zealand and North America. Details of the 45WH can be found in Gorman *et al.* (2010) and Godoi *et al.* (2016).

Modelled time series of significant wave height (H_s) were extracted from the 45WH at the 418 model grid points on the 200 m isobath around New Zealand (Figure 1) for the 44-year period 1958–2001. A range of H_s thresholds has been selected in the literature to define storm waves (Ferreira, 2005), usually based on the wave climate of the study region. As different wave climates are found along the New Zealand coastline (Godoi *et al.*, 2016, 2017), H_s thresholds should vary accordingly. A simple way of obtaining H_s thresholds that match the local wave climate is to select them based on percentiles rather than establishing a single value for the whole study region. Thus, storm wave events were identified using the peaks-over-threshold (POT) approach considering the 95th percentile threshold of each site. In other words, H_s maxima from independent storms were obtained when they were above the 95th percentile of the time series, following, e.g. Phillips *et al.* (2015) and Harley *et al.* (2009). A timeframe also needs to be considered for ensuring independence between storms,

because successive H_s peaks occurring in a short interval are likely to be part of the same event. To this end, H_s maxima were selected only when they occurred at least 72 h apart. The 72-h interval was motivated by past studies where 72 h is the time lag below which the storms are autocorrelated (Mathiesen *et al.*, 1994; Lopatoukhin *et al.*, 2000). This is a well-established threshold in the literature, used in the identification of both storm and extreme waves (Alves and Young, 2003; Méndez *et al.*, 2006; Stephens and Gorman, 2006; Godoi *et al.*, 2017).

Here, we aim at understanding some general characteristics of SWCs around the whole coastline of New Zealand. This is unlikely to be accomplished with the implementation of the techniques discussed in the previous section because they require beach recovery periods to be defined. Therefore, a simple and objective criterion has been chosen to assess storm wave clustering without considering erosion processes and recovery periods of individual beaches. This criterion is based on the assessment of the index of dispersion (I_d) of time intervals between storm peaks.

The I_d is a measure of the normal variability of intervals between storm peaks and is the quantity (with time dimension) defined as the ratio of the variance ($\Delta T - \langle \Delta T \rangle$)² of the time interval ΔT between storm peaks to the mean interval $\langle \Delta T \rangle$. The method itself is not innovative, because it has been applied by other authors (Mailier *et al.*, 2006; Kvamstø *et al.*, 2008; Vitolo *et al.*, 2009) in different contexts and using different approaches. However, the way the method has been employed here differs from previous work. Two assumptions were made in order to select appropriate values for the time interval between storm peaks used for grouping storms into clusters. This interval needed to be short enough to be considerably lower than both the I_d value and the mean interval at each location analysed, and long enough to allow SWCs to be identified. Values of $0.5I_d$ were found to satisfy both requirements for all time series of storm wave occurrence assessed, as shown in Figure 2(a). Hence, they have been adopted in this work, and storms were grouped into clusters when the time interval between them was shorter than $0.5I_d$. Sensitivity tests for intervals equal to $0.4I_d$ and $0.6I_d$ were also conducted to verify the variability of the overall mean of the number of SWCs in the study region during the period 1958–2001 (not shown). The overall mean values did not change considerably (133.8, 140.7, and 139.9 for $0.4I_d$, $0.5I_d$, and $0.6I_d$, respectively) because SWCs became generally longer rather than more numerous when the intervals increased, whereas the number of SWCs only slightly reduced when the intervals were shortened. So, our original choice ($0.5I_d$) was kept. Values of $0.5I_d$ varied between 9.7 and 25.4 days, with an average of 15.1 days among all sites. Although the beach recovery period is not a key factor in the determination of SWCs in our analysis, values of $0.5I_d$ were found to be within the range of beach recovery periods proposed in the literature (Birkemeier *et al.*, 1999; Ferreira, 2005; Almeida *et al.*, 2012; Karunaratna *et al.*, 2014). Figure 2(a) shows the values of $0.5I_d$ (dashed line), the mean interval (solid line), and the standard deviation of the time interval (dotted line) calculated for each

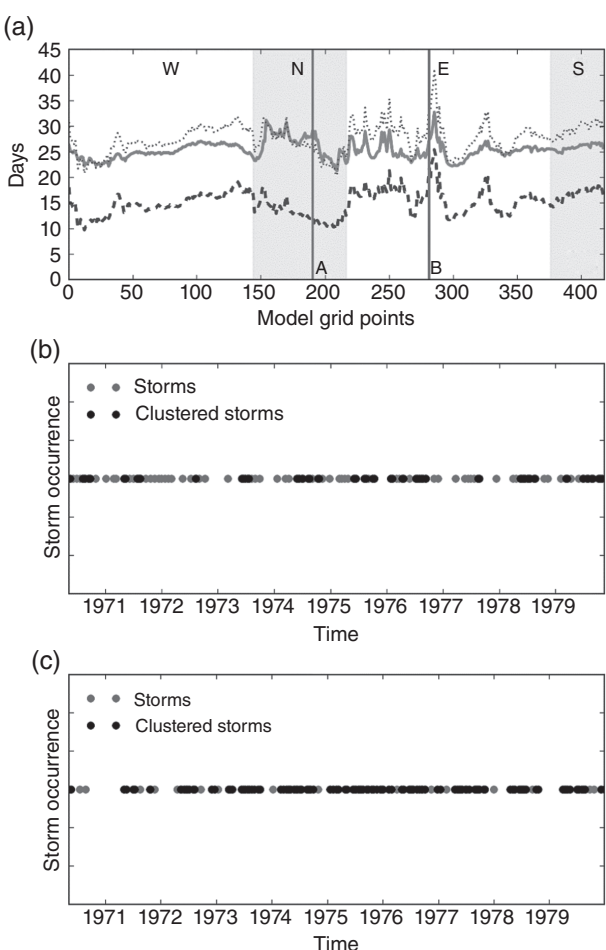


Figure 2. (a) Statistics computed for time series of storm wave occurrence at the 418 model grid points on the 200 m isobath: half of the index of dispersion of time intervals between storm peaks (dashed line), mean interval between storm peaks (solid line), and standard deviation of the time interval between storm peaks (dotted line). Vertical lines A and B mark the largest and smallest differences between the mean interval between storm peaks and half of the index of dispersion; the locations of the model grid points associated with these differences are displayed in Figure 1 as A and B. W, N, E, and S stand for west, north, east, and south, respectively, delimited according to Figure 1. Shaded and non-shaded areas of the graph comprise the model grid points along each section of the coastline (W: 0–143; N: 144–216; E: 217–375; S: 376–417), with 0 being located on the southwestern coast (triangle in Figure 1) and the subsequent numbers follow a clockwise rotation; (b) time series of occurrence of storms and clustered storms at site A; (c) time series of occurrence of storms and clustered storms at site B. Grey circles represent storm waves, whereas black circles indicate storm waves pertaining to clusters.

of the 418 model grid points on the 200 m isobath over the period 1958–2001. The standard deviation of the time interval between storm peaks was plotted instead of its variance to allow better visualization of the values of the other curves. One notes that the values of the standard deviation were generally closer to the mean values on the north coast than on the other coasts (Figure 2(a)). This indicates a smaller variability in storm occurrence (more consistent wave climate) on the north coast than on the others, which results from a typically low-energy wave environment on the north coast that is regularly disturbed by tropical cyclone-generated waves in summer (Godoi *et al.*,

2016). Examples of clustering at sites A and B (Figure 1) during the 1970s are displayed in Figures 2(b) and (c), respectively. The examples show the temporal distribution of clustered and non-clustered storm occurrences identified at the sites with the largest (site A) and smallest (site B) differences (16.6 and 5.5 days) between the mean interval between storm peaks and $0.5I_d$. By using this approach, for two sites with the same mean interval between storm peaks, the one with a less consistent wave climate (larger variability in the time interval between storm peaks) will have a higher I_d value and, consequently, more clustered storms. In this case, a higher I_d means a higher chance of erosion or any other cluster-induced damage as well as a higher chance of multi-hazard effects, because the longer duration of SWCs relative to individual storms will mean that conditions will be more likely to coincide with a high tide.

Although the focus of this article is not on beach processes, such as erosion and sediment transport, two measures, based on offshore H_s and storm duration (period in which H_s remained above the 95th percentile), were used to provide an overview of the potential for coastal erosion. These were the average CSE per cluster and average storm power index (SPI) per cluster. Both the CSE (Mendoza and Jimenez, 2006; Harley *et al.*, 2009, 2010; Phillips *et al.*, 2015) and SPI (Dolan and Davis, 1994; Karunaratne *et al.*, 2014) were first calculated for each storm. To do so, the formulae presented by Harley *et al.* (2010) and Karunaratne *et al.* (2014) were employed here (Equations (1) and (2), respectively); where ρ is the mass density of sea water (1025 kg m^{-3}), g is the gravitational acceleration (9.8 m s^{-2}), Δt is the temporal resolution of the data set (1 h), N is the total number of H_s values i above the 95th percentile during the storm, $H_{s_{\max}}$ is the storm peak H_s value, and D is the storm duration. The cumulative effect of all storms pertaining to a single cluster was determined by summing up their respective CSE/SPI values. Lastly, the cumulative energy obtained for all SWCs of each site on the 200 m isobath was temporally averaged over the period 1958–2001. The SPI overestimates the energy content of a storm because it only considers the maximum H_s (Mendoza and Jimenez, 2006). Conversely, H_s of each recording time during a storm is used in the computation of the CSE. Nonetheless, for the sake of the ability to compare to studies that have applied the SPI, this is also calculated here.

$$\text{CSE} = \frac{1}{16} \rho g \Delta t \sum_{i=1}^N H_{s_i}^2 \quad (1)$$

$$\text{SPI} = H_{s_{\max}}^2 D \quad (2)$$

To verify changes in SWCs over the period 1958–2001, trends in annual averages of SWC parameters (number of storms within the cluster, CSE, and cluster duration) were calculated using the Mann–Kendall test (Mann, 1945; Kendall, 1955) and the Theil–Sen estimator (Theil, 1950; Sen, 1968). The Mann–Kendall test was employed to estimate monotonic upwards/downwards trends, while

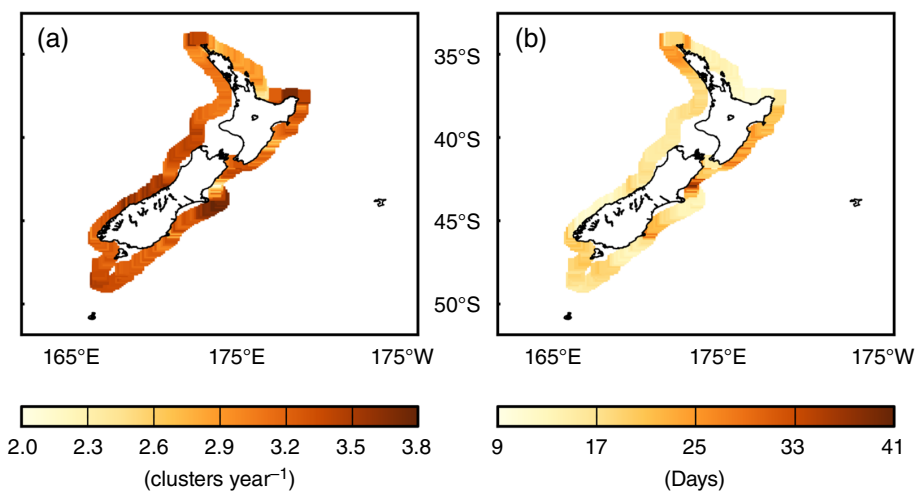


Figure 3. Considering the period 1958–2001: (a) annual average number of SWCs; (b) average SWC duration. The averages were calculated at the model grid points on the 200 m isobath.

the Theil–Sen estimator was used to calculate the slope (magnitude) of the trends. Trends were computed for three time periods: the pre-satellite (1958–1978) and satellite (1979–2001) eras spanned by the data set, and a long-term period (1958–2001). Statistical significance of trends was assessed using *p*-value.

Storm wave clustering during different phases of the ENSO, IOD, SAM, PDO, and ZW3 was investigated through correlations of the climate pattern indices (Southern Oscillation Index (SOI), Dipole Mode Index (DMI), SAMI, PDO Index, and ZW3 Index) with storm cluster indices (explained below) and SWC parameters. Monthly climate indices were sourced from the National Oceanic and Atmospheric Administration (NOAA), Japan Agency for Marine-Earth Science and Technology (JAMSTEC), British Antarctic Survey (BAS), Japan Meteorological Agency (JMA), and Raphael (2004), respectively. Except for the ZW3 Index, which is available only from 1979, all the other climate indices were collected for the period 1958–2001. In order to perform the correlations, a monthly storm cluster index was created for every location analysed by assigning weights to each month based on the number of clustered storms within that month. First, the number of storms in each month of the 44-year period was found using the POT approach and the 72-h interval, and those that were clustered were identified using the index of dispersion (as described above). This resulted in two time series, a monthly time series of the number of storms and a monthly time series of the number of clustered storms. Then, the latter was divided by the former yielding a monthly storm cluster index. The same procedure was carried out for the 418 sites on the 200 m isobath. Then, correlations of monthly anomalies between the storm cluster indices and climate indices were performed. Additionally, seasonally averaged monthly anomalies of storm cluster indices were correlated with both seasonal and lagged-seasonal (1-season lag) averages of monthly anomalies of climate indices. Lastly, correlations of annually averaged

monthly anomalies between SWC parameters (number of storms within the cluster, CSE, and cluster duration) and climate indices were carried out. Correlations were performed using the Pearson's correlation coefficient (*R*). As demonstrated by Godoi *et al.* (2016, 2017) and Pickrill and Mitchell (1979), the mean and extreme wave climates around New Zealand can be classified into four main wave climates according to their exposure to wave generation zones. Thus, four model grid points on the 200 m isobath (48.469°S/166.375°E, 39.188°S/172.375°E, 36.094°S/176.000°E, and 41.625°S/175.375°E), corresponding to the major coastline orientations (Figure 1), were selected so that correlations of monthly anomalies between their storm cluster indices and climatic indices could be computed at several timescales using the squared wavelet coherence spectra.

2.1. Overview of storm wave clustering around New Zealand

SWCs were most frequently observed to the northeast of New Zealand and on the central eastern coast of the South Island (Figure 3(a)), where approximately four SWCs occurred per year. Karunarathna *et al.* (2014) identified 80 SWCs at Narrabeen Beach between 1981 and 2000, resulting in four SWCs per year on average. Their results are comparable to our sites with largest occurrences of SWCs (the authors note SWCs are fairly common at Narrabeen Beach).

A secondary maximum in cluster occurrence was experienced on the central western coast of the South Island. This agrees with the extreme wave conditions documented by Godoi *et al.* (2017), who showed that extreme waves are more closely spaced in this region and on the northeastern coast than in other regions around the country. A common feature between these two regions is that swells from the south quadrant undergo considerable refraction prior to arriving at the coast. SWCs had generally longer durations on the east coast than on the other coasts (Figure 3(b)). They were least frequent (Figure 3(a)) where they lasted

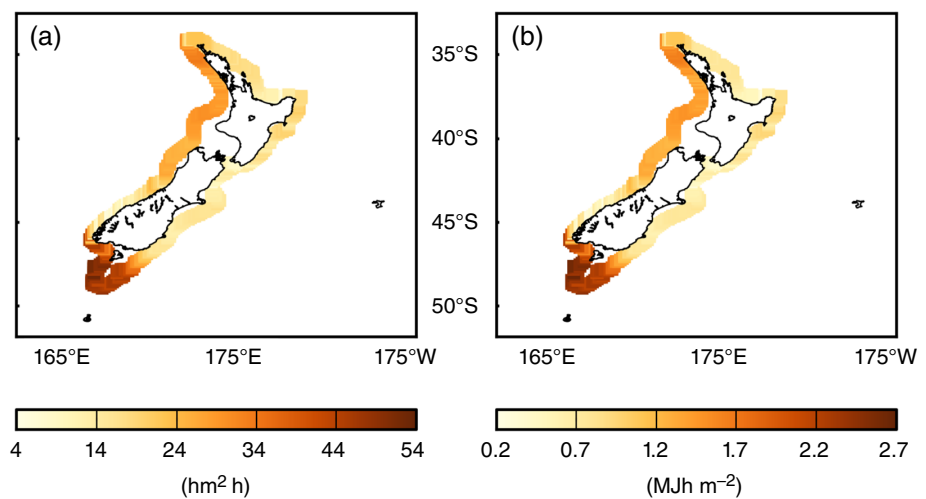


Figure 4. Measures of the potential for cluster-induced coastal erosion: (a) average SPI per cluster (in hecto $\text{m}^2 \text{h}$); (b) average CSE per cluster (in mega Jh m^{-2}). The averages were calculated using all SWCs occurred during the period 1958–2001 for each model grid point on the 200 m isobath.

longest (Figure 3(b)), up to about 40 days on average, as can be noted to the north of the large peninsula on the central eastern coast of the South Island. This segment of the coastline is sheltered from the main swell direction (SW) and presents a relatively low-energy wave climate (Godoi *et al.*, 2016, 2017).

As expected, both the average CSE per cluster and average SPI per cluster (Figure 4) showed a similar spatial distribution of potential for cluster-induced coastal erosion. These results highlight the regions around the country where SWCs played the most critical role in terms of coastal hazards, which were southern New Zealand followed by the west coast of the North Island. This is directly related to the intense activity of southwesterly swells generated by recurrent extratropical cyclones (Sinclair, 1995). Karunarathna *et al.* (2014) obtained values between 2.86 and 73.83 $\text{hm}^2 \text{h}$ for the SPI per cluster for events representative of the scale of beach profile change at Narrabeen Beach. Their range was 45.4% larger than ours ($4.17\text{--}52.99 \text{ hm}^2 \text{h}$). Regarding the average CSE values per cluster, 59% of the sites we investigated were less than 1.19 MJh m^{-2} , while 12% were in the most hazardous condition range ($2.17\text{--}2.67 \text{ MJh m}^{-2}$) (Figure 4(b)).

The 45WH was carried out using reanalysed data from ERA-40 as boundary conditions. The quantity and quality of such data vary in time, and this may produce spurious trends. Under these circumstances, the well-known temporal inhomogeneity issue, concerning the introduction of satellite data to the reanalysis data set (Bromwich and Fogt, 2004), was explored by evaluating trends for different periods. Contrasting results were obtained when trends in SWC parameters were calculated for the pre-satellite (1958–1978) and satellite (1979–2001) eras (Figure 5, left and middle columns, respectively). Trends were generally positive during the pre-satellite period and negative during the satellite period, although only a low percentage of the analysed sites had statistically significant results [7.42% (4.31%) of the sites showed statistically significant results for trends in CSE during the period 1979–2001

(1958–1978), while the percentages were even lower for trends in the other parameters]. Note that opposing trends were generally observed at different locations, suggesting that these can also be due to different climate conditions in the two periods rather than due to data inhomogeneity in the reanalysis. By using only satellite data over the period 1985–2008, Young *et al.* (2011) detected only positive trends in the 99th percentile H_s in the region around New Zealand.

When trends were calculated for the period 1958–2001 (Figure 5, right column), only positive trends were identified, in which case SWCs have become more hazardous, have lasted longer, and have incorporated more storms. Trends were mostly observed around the South Island, with only a few locations along the North Island (the northernmost and southernmost tips) with statistically significant trends for all parameters (Figure 5, right column). Nevertheless, several sites off the central western coast of the North Island also showed notable trends in cluster duration and in the number of storms within the cluster. Southern New Zealand is not only where the highest potential for cluster-induced coastal erosion was found (Figure 4), but also where its largest trends were detected (Figure 5, right column, first row). At some sites in this region, trends might result merely from increasing wave heights (Godoi *et al.*, 2016) and/or changes in wave direction (Hemer *et al.*, 2010), while at other sites, they were associated with an increasing number of storms within the cluster (Figure 5, right column, third row). For the same period (1958–2001), positive trends in the mean H_s were reported for southern New Zealand (Godoi *et al.*, 2016), whereas no trends in extreme waves (maxima H_s above the 99th percentile from independent storms) were observed (Godoi *et al.*, 2017). On the other hand, trends in extreme waves were found along the southeastern coast (Godoi *et al.*, 2017), where increasing trends in energy content, cluster duration, and in the number of storms within the cluster were also detected (Figure 5, right column). Increases in intensity of cyclones

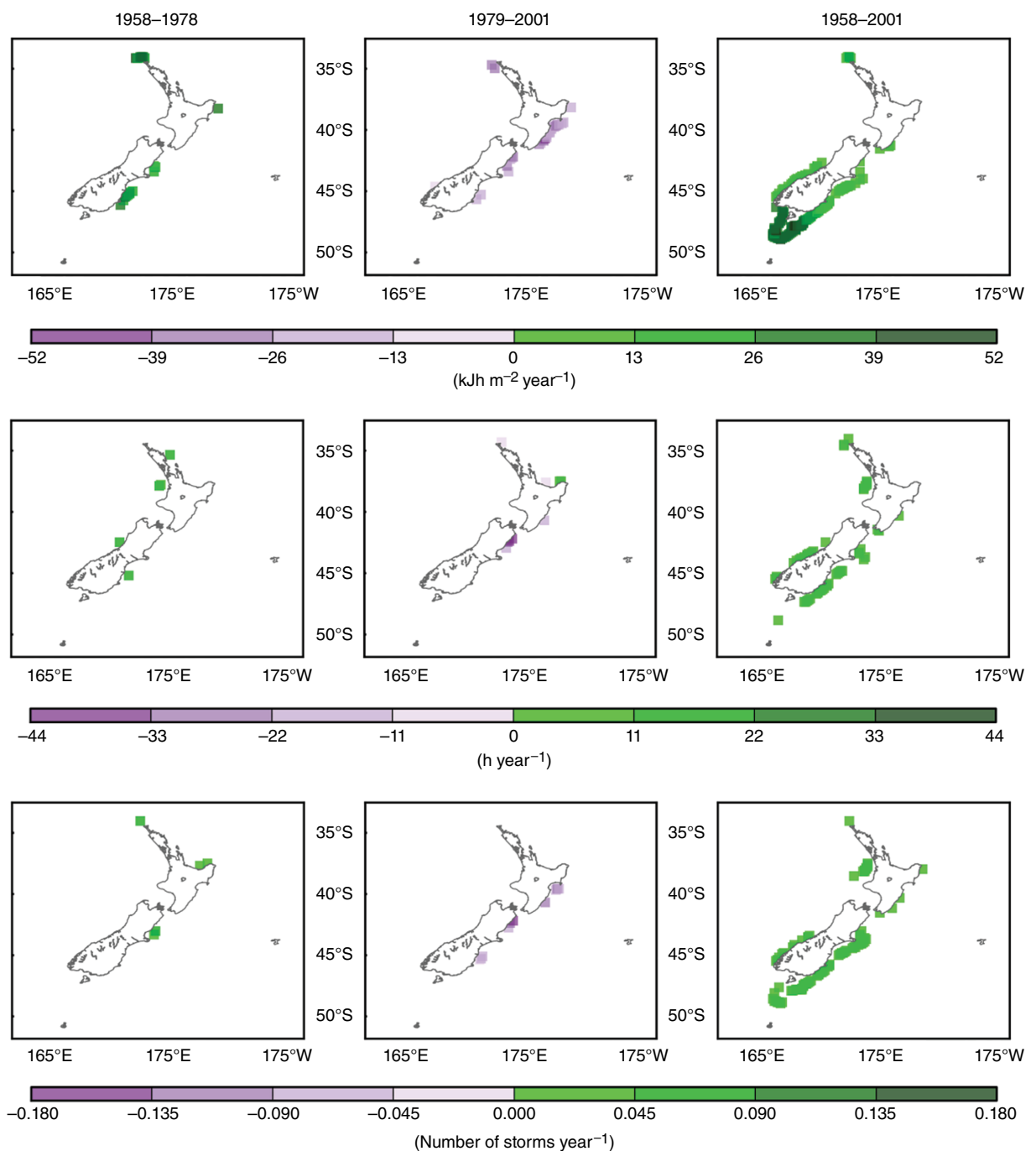


Figure 5. Monotonic trends in SWC parameters, calculated for the pre-satellite period (1958–1978, left column), satellite period (1979–2001, middle column), and long-term period (1958–2001, right column). Top row: CSE (in kilo Jh m^{-2}); middle row: cluster duration; bottom row: number of storms within the cluster. Trends were calculated from annual averages of the cluster parameters using the Mann–Kendall test and the Theil–Sen estimator. Only statistically significant values at the 95% confidence level (calculated using p -value) are displayed.

in the Tasman Sea (Simmonds and Keay, 2000) are likely related to the trends in the SWC parameters observed on the west coast of the South Island (Figure 5, right column). The latter, however, contradict the trends in directional distribution of waves, which indicate a reduction in northwesterly and westerly waves arriving on this coast (Hemer *et al.*, 2010). The contrasting results between the pre-satellite and satellite eras do not allow us to provide robust detection of the long-term trends.

Nonetheless, trends were computed using results from a wave hindcast forced by ERA-40 data, which in turn were found to be suitable for analysing the recent trend in the SAM, at least as far back as 1973 (Marshall, 2003). This provides additional confidence in the long-term trends, because the main signature of the SAM takes place in the high and mid-latitudes of the Southern Hemisphere, where the waves that consistently affect New Zealand are generated.

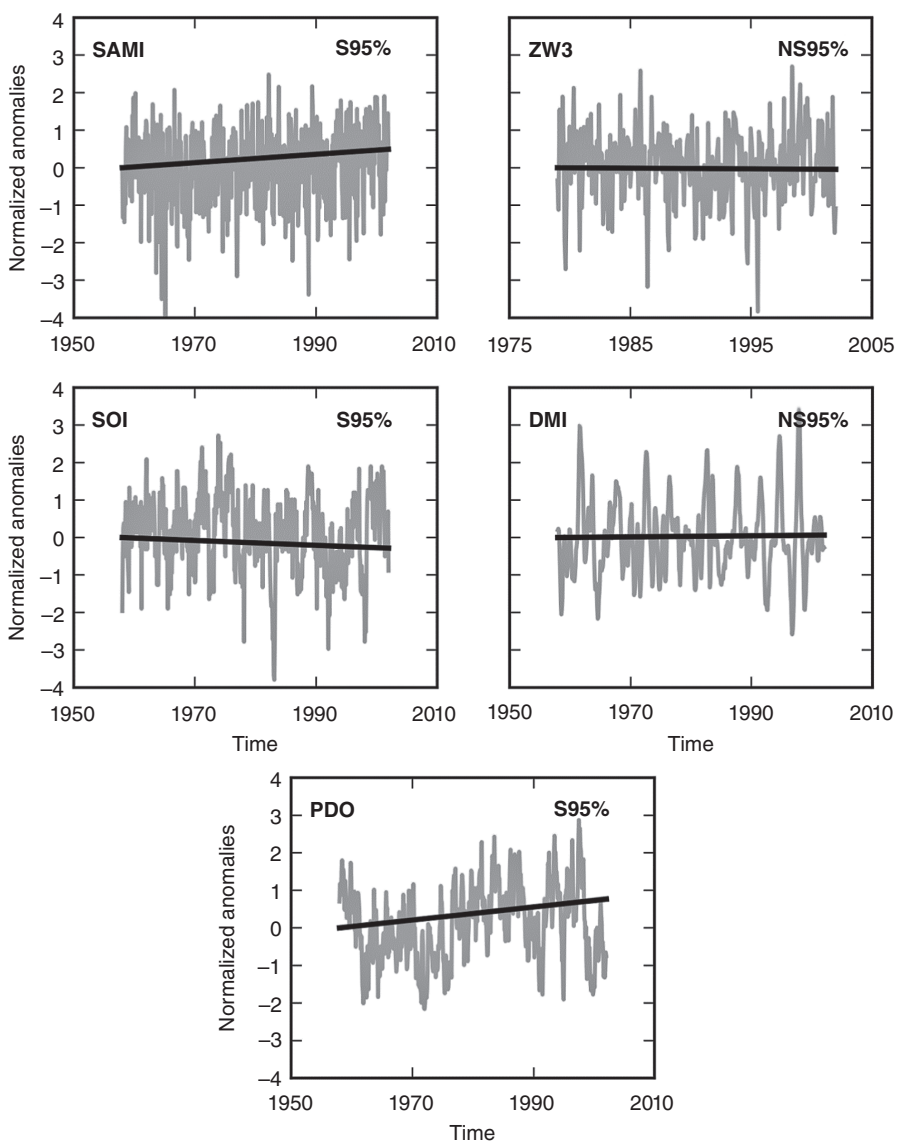


Figure 6. Monotonic trends in normalized anomalies of climate indices: SAMI, ZW3 Index, SOI, DMI, and PDO Index. The anomalies of climate indices were normalized by the standard deviation. Trends were computed for the period 1979–2001 for the ZW3 Index, and for the period 1958–2001 for the other indices. S95% and NS95% stand for statistically significant and non-significant at the 95% confidence level, respectively.

Trends for a negative SOI after 1976 (Trenberth and Hoar, 1996), for a positive SAM since the mid-1960s (Marshall, 2003), and for a positive PDO since mid-1970s (Pezza *et al.*, 2007) have been documented. These were also verified here for the period 1958–2001 (Figure 6) and are in agreement with increases in SWC parameters (as discussed in the next section). The long-term trends identified in those climatic indices only explain a small portion of the variance, which is, for many purposes, less important than the short-term variability. However, when dealing with coastal hazards and flooding, even a small long-term change in storms and extreme events will potentially lead to increased damage.

2.2. Association between climate patterns and storm wave clustering

Monthly and lagged-seasonal correlations between storm cluster indices and climate indices are presented in

Figures 7 and 8. Seasonal correlations did not provide significant additional information in relation to the monthly and lagged-seasonal ones, and therefore their results are not shown. Statistically significant correlations were found at many sites along the 200 m isobath around New Zealand, albeit clustered storms were generally weakly correlated ($|R| < 0.42$) with climate indices.

With respect to monthly correlations (Figure 7), fewer clustered storms occurred on the west coast in association with positive SAM. The strengthening of the circumpolar westerlies is characteristic of a positive SAM (Marshall, 2003; Gupta and England, 2007), and so one would expect the opposite response in the number of clustered storms. Nevertheless, a polewards shift of extratropical cyclone storm tracks has been observed (Gillett and Thompson, 2003), accompanying the trend towards the positive phase of the SAM since the mid-1960s (Marshall, 2003). This shift results in decreases in westerly

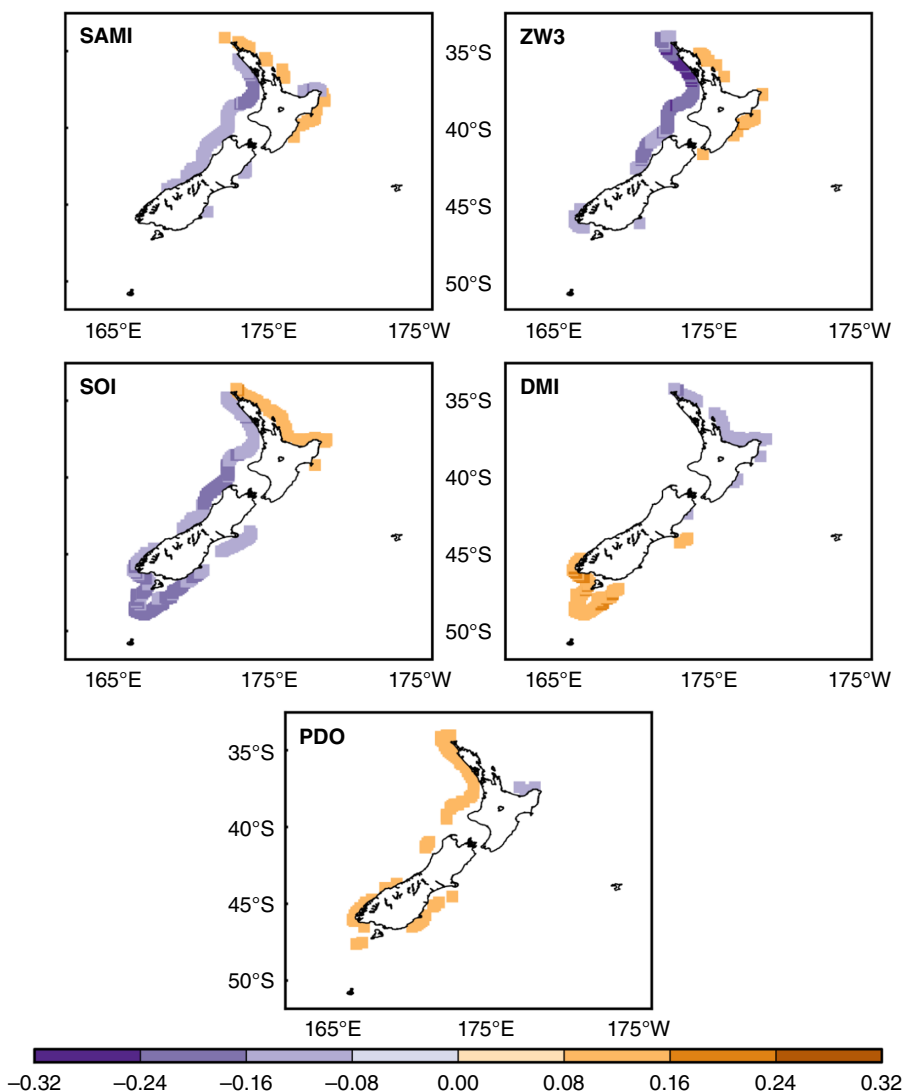


Figure 7. Correlations of monthly anomalies between storm cluster indices and climate indices. Correlations were carried out at the model grid points on the 200 m isobath over the period 1958–2001 for the SAMI, SOI, DMI, and PDO Index, and over the period 1979–2001 for the ZW3 Index. Only statistically significant values at the 95% confidence level are displayed.

waves in the regions immediately adjacent to the west coast (Hemer *et al.*, 2010) because of a southwards displacement of wave generation zones (Godoi *et al.*, 2017). Consequently, the wave energy coming from the west is reduced on the west coast when the positive phase of the SAM is more pronounced. On the contrary, the number of clustered storms increased on the same coast during negative phases of the ZW3, due to the intensification of the eastwards atmospheric zonal flow. The latter becomes more relevant in the lower latitudes of the study region, as demonstrated by strengthened correlations northwards (Figure 7). The west coast was also affected by SWCs generated during opposite phases of the PDO (positive) and ENSO (negative, El Niño events). Likewise, clustering was more frequent during positive IOD and negative ENSO to the south of New Zealand. The IOD can take place through the ENSO conditions because of the teleconnecting nature of these two modes (Schott *et al.*, 2009; Izumo *et al.*, 2010; Taschetto *et al.*, 2011; Godoi *et al.*,

2016). The signature of this relationship was also observed along the north coast, with enhanced clustering during La Niña events (positive ENSO) and negative IOD. Clustered storms occurred more frequently on the east coast of the North Island during positive phases of the SAM and ZW3, and on the east coast of the South Island during negative ENSO and positive PDO. During positive SAM, the refraction of westerly swells seems to make waves arrive on the east coast of the North Island with more intensity than on the same coast of the South Island (Godoi *et al.*, 2016, 2017). In a similar fashion, the waves produced by the northwards wind stress anomaly to the south of New Zealand related to positive ZW3 (Cai *et al.*, 1999) have a more marked effect on the North Island than on the South Island. Conversely, the larger southwesterly waves generated to the south of New Zealand during negative ENSO and positive PDO (Godoi *et al.*, 2016) have a stronger influence on the east coast of the South Island. Given that the main signatures of the ENSO, IOD, and PDO

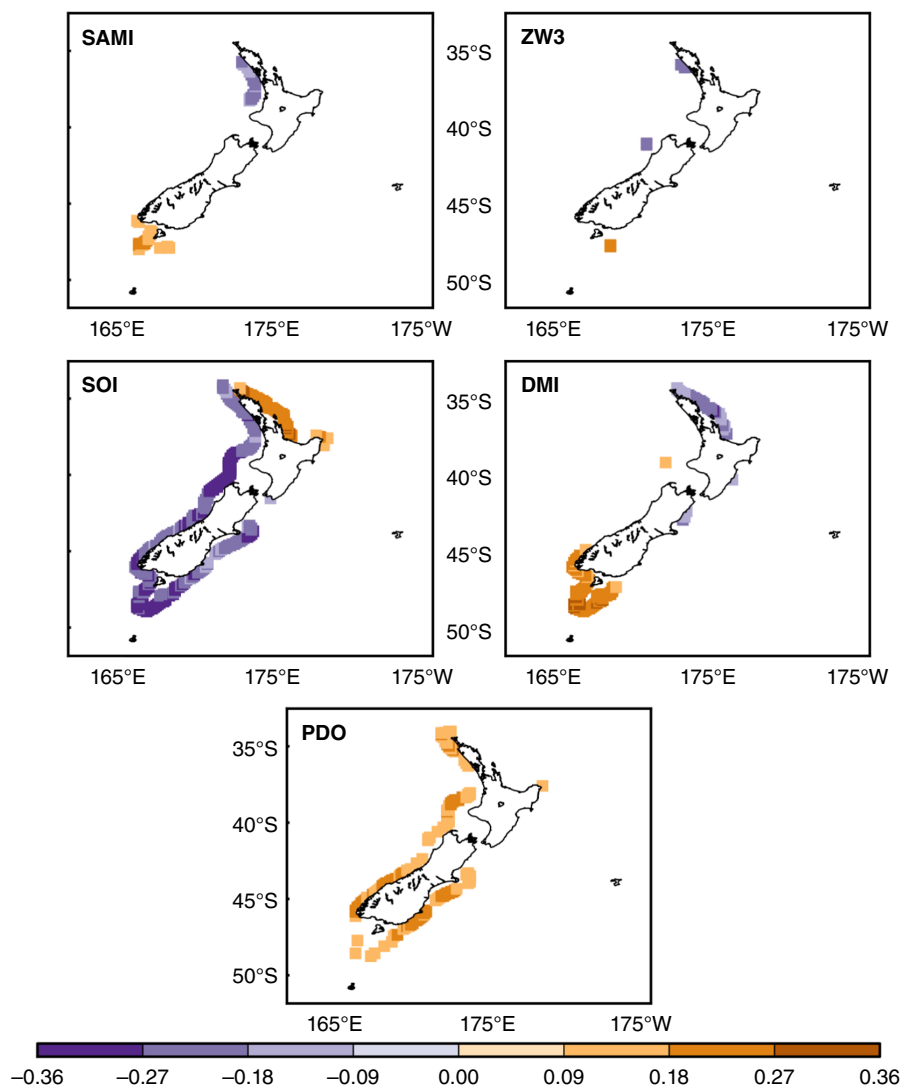


Figure 8. Correlations of seasonally averaged monthly anomalies between storm cluster indices and climate indices lagged by one season. Correlations were carried out at the model grid points on the 200 m isobath over the period 1958–2001 for the SAMI, SOI, DMI, and PDO Index, and over the period 1979–2001 for the ZW3 Index. Only statistically significant values at the 95% confidence level are displayed.

are observed far away from New Zealand, their associated conditions modify the atmosphere and ocean around the country through teleconnections. Tropic–extratropic teleconnections occur through disturbances in the Hadley cell (Liu and Alexander, 2007). The latter modifies the subtropical atmospheric circulation by changing the moisture and heat sources responsible for dispersion of the Rossby waves that influence the extratropics (Grimm and Ambrizzi, 2009). As Rossby waves are dispersed, cyclone and anti-cyclone winds strengthen. Anomalously strong winds generate larger waves, resulting in more frequent storm waves. As the time between consecutive storms shortens, in this case, more clustered storms are observed.

The first signature of the ENSO is generally observed in the eastern equatorial Pacific (Bjerknes, 1966; Wyrtki, 1975; Trenberth and Hoar, 1996), and therefore, the ENSO-related changes in the atmosphere and ocean around New Zealand are delayed. Because of the inherent noisiness of the SOI time series at short timescales,

seasonally averaged SOI values have been found to be more suitable for correlations than monthly averaged values (Harley *et al.*, 2010). Hence, lagged-seasonal correlations are likely to be better for assessing variations in storm wave clustering around New Zealand related to the ENSO fluctuations. The same is true for the IOD and PDO conditions, which are also strongly influenced by the ENSO variability (Mantua *et al.*, 1997; Schott *et al.*, 2009). Although New Zealand is situated in the latitude band where the largest variabilities related to the SAM and ZW3 are experienced (the high and mid-latitudes of the Southern Hemisphere), lagged-seasonal correlations were also performed for these oscillations. Thus, climate patterns of a given season were correlated with clustered storms of the next season. Correlations with the SOI strengthened substantially along all coasts (Figure 8). A similar pattern was observed for the DMI to the south of New Zealand, along the southwestern coast, and in part of the north coast, and for the PDO Index at most sites

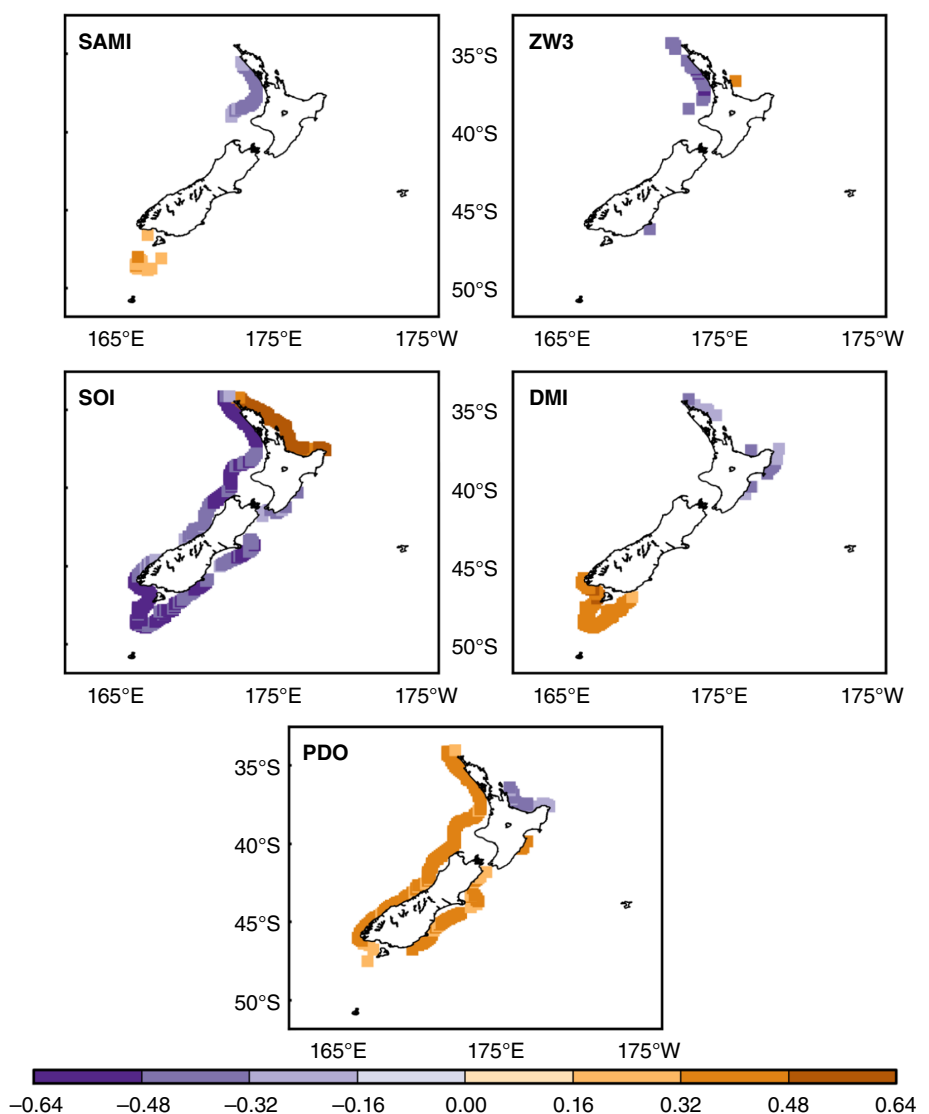


Figure 9. Correlations of annually averaged monthly anomalies between CSE per cluster and climate indices. Correlations were carried out at the model grid points on the 200 m isobath over the period 1958–2001 for the SAMI, SOI, DMI, and PDO Index, and over the period 1979–2001 for the ZW3 Index. Only statistically significant values at the 95% confidence level are displayed.

where statistically significant monthly positive correlations had been obtained. This enhancement relative to non-lagged correlation is due to the time that teleconnected phenomena take to respond to the warming and cooling of the Indian and Pacific Oceans' tropical waters. An example of this delayed response is the warming in the tropical Indian Ocean caused by the ENSO-related fluctuations, which takes approximately 3–6 months to occur (Deser *et al.*, 2010). As opposed to the results for the SOI, DMI, and PDO Index, lagged-seasonal correlations between clustered storms and SAMI/ZW3 Index either weakened or lost statistical significance at most sites where significant monthly correlations had been obtained, with the exception of the positive correlations with the SAMI found now to the south of New Zealand (Figure 8). These results demonstrate that the SWCs that hit New Zealand are more synchronized with the SAM and ZW3 fluctuations than with those of the ENSO, IOD, and PDO. Seasonal correlations (not shown) showed slightly higher

absolute values (up to $|R|=0.42$) than the monthly and lagged-seasonal ones for the SAMI, on the west coast, and for the ZW3 Index, at a few sites on the north and east coasts.

SWC parameters had a stronger connection with the ENSO and PDO than the other oscillations (Figures 9–11). Although the north coast is generally impacted by relatively low-energy SWCs (Figure 4), their CSE was highly correlated (R up to 0.64) with La Niña episodes (Figure 9). During such episodes, stronger northeasterly winds are produced to the north of New Zealand (Gorman *et al.*, 2003), leading to larger waves on the north coast (Gorman *et al.*, 2003; Godoi *et al.*, 2016). La Niña-like effects also occur during negative PDO because of its inverse relationship with the ENSO (Godoi *et al.*, 2016), and this resulted in more energetic SWCs along part of the north coast (Figure 9). Not surprisingly, El Niño-like effects are experienced during positive PDO (Mantua *et al.*, 1997) on the west, south, and east coasts,

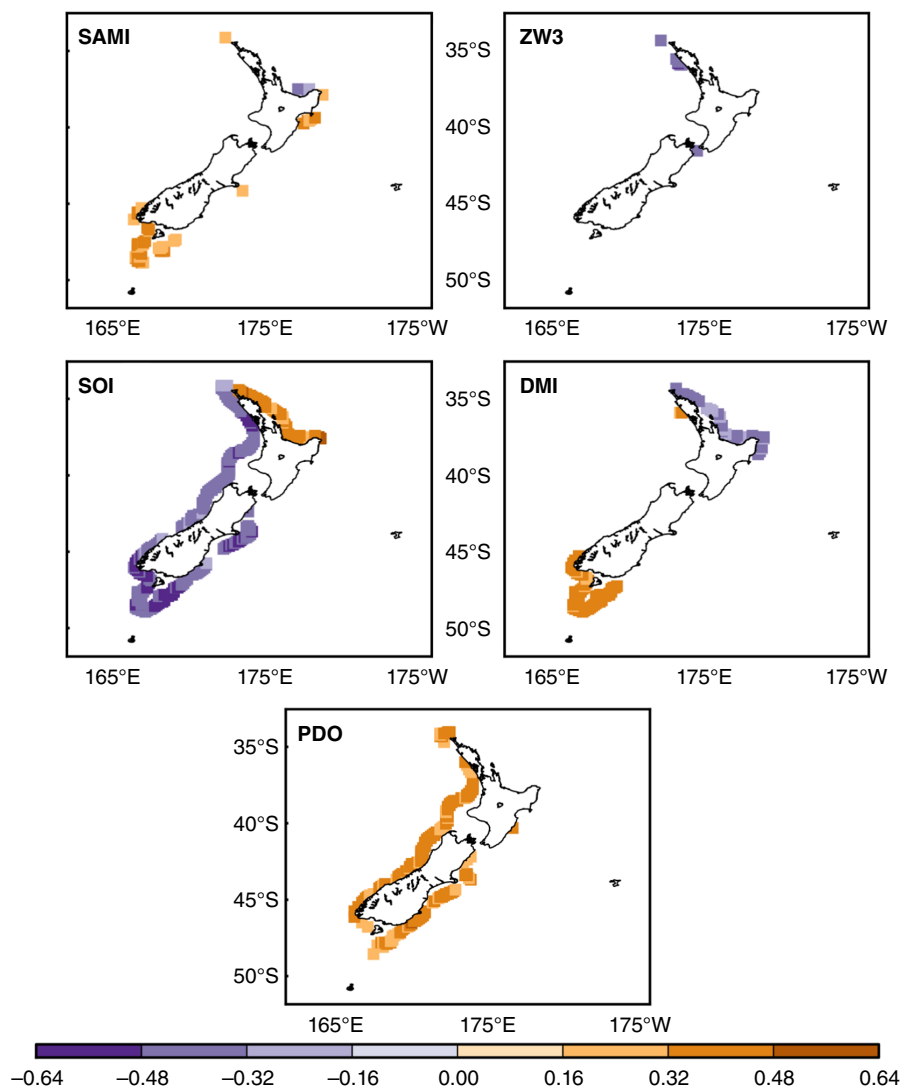


Figure 10. Correlations of annually averaged monthly anomalies between storm cluster duration and climate indices. Correlations were carried out at the model grid points on the 200 m isobath over the period 1958–2001 for the SAMI, SOI, DMI, and PDO Index, and over the period 1979–2001 for the ZW3 Index. Only statistically significant values at the 95% confidence level are displayed.

and entail increased southwesterly winds (Gordon, 1986) and correspondingly larger waves (Laing, 2000). This explains the strong correlations of CSE with the SOI and PDO Index along those coasts (Figure 9). SWCs were also more energetic on the west coast of the North Island during negative phases of the SAM and ZW3, and to the south of New Zealand during positive phases of the SAM and IOD (Figure 9). SWCs tended to last longer along most of the west, south, and east coasts during positive PDO and negative ENSO, while their duration increased on the north coast during La Niña and La Niña-like (negative IOD) events (Figure 10). Positive phases of the SAM and IOD (stronger westerly and southwesterly winds, respectively) occurred when there were longer-lasting SWCs to the south of New Zealand. A larger number of storms within the cluster coincided with El Niño episodes and positive PDO along the west and east coasts, and with La Niña events and negative IOD on the north coast (Figure 11). The number of storms was also larger on the

west coast during negative SAM and in the presence of a more intense zonal flow during negative ZW3, while in southern New Zealand the number of storms increased during El Niño conditions and positive phases of the SAM and IOD. These annual correlations (Figures 9–11) support the assumption that trends in SWC parameters (Figure 5) are associated with trends in climate oscillations (Figure 6). More frequent El Niño-like conditions, during either negative ENSO or positive PDO phases, were consistent with increases in SWC parameters on the south, east, and west coasts of the South Island. Furthermore, strengthened circumpolar westerlies associated with the trend for a positive SAM (Marshall, 2003) were compatible with trends in SWC parameters to the south of New Zealand.

Figure 12 is an example of the wavelet spectral analysis results obtained for the four model grid points (Figure 1) selected as representative of the major coastline orientations, north (N), west (W), east (E), and south (S). It

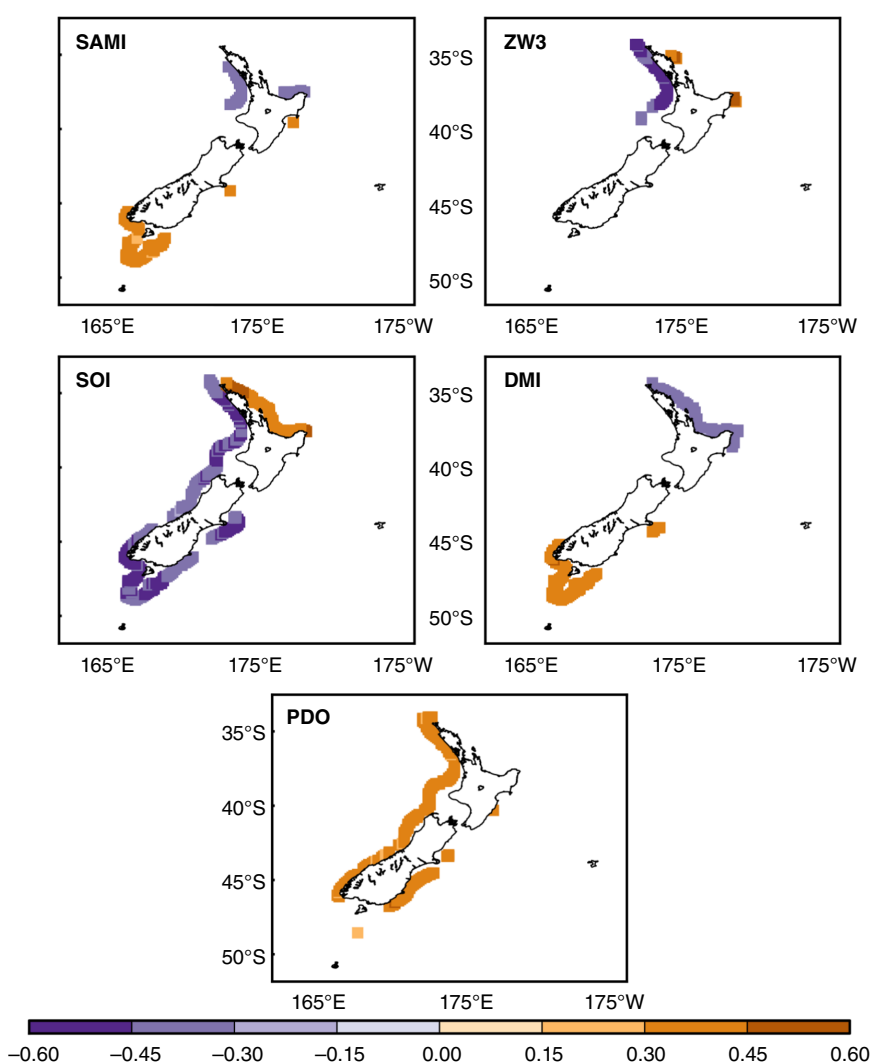


Figure 11. Correlations of annually averaged monthly anomalies between the number of storms within the cluster and climate indices. Correlations were carried out at the model grid points on the 200 m isobath over the period 1958–2001 for the SAMI, SOI, DMI, and PDO Index, and over the period 1979–2001 for the ZW3 Index. Only statistically significant values at the 95% confidence level are displayed.

illustrates the correlations of monthly anomalies between storm cluster indices and the SOI at several timescales, and highlights the periods in which the ENSO conditions were presumably related to the number of clustered storms around New Zealand. The most relevant signals were generally observed at 2–7 year timescales. On the north coast, increased northeasterly winds, typical of La Niña events, were responsible for a more frequent clustering from the late 1960s to the late 1980s (Figure 12, top). Clustered storms were most correlated with positive SOI during the early and mid-1970s, coinciding with the 1974–1976 La Niña (Jury *et al.*, 2002). Curiously, the extreme 1998–1999 La Niña (Cai *et al.*, 2015) did not seem to have had any relation to storm wave clustering on the north coast, as opposed to the extreme La Niña of 1988–1989 (Cai *et al.*, 2015) (upwards arrows, 4-year cycle). Increases in clustered storms due to stronger southwesterly winds during El Niño events were more pronounced on the west coast, with strongest correlations in the early 1980s (Figure 12, left). An extreme El Niño

indeed occurred in 1982–1983 (Wang and Cai, 2013; Cai *et al.*, 2014). The long horizontal band of strong correlations during almost the whole period of analysis (Figure 12, left) also comprises two other extreme El Niño events, occurred in 1972–1973 (Saji *et al.*, 1999) and 1997–1998 (Wang and Cai, 2013; Cai *et al.*, 2014), as well as the consecutive 1986–1987 and 1987–1988 El Niño episodes (Cai *et al.*, 2015), and the 1991–1992 El Niño, which was only short and ended abruptly (Hayward, 1993). A 2-year cycle associated with the early 1960s El Niño (McPhaden *et al.*, 2015) showed a strong correlation with clustered storms to the south of New Zealand (Figure 12, bottom). El Niño was also related to clustering on the east coast from the early 1960s to the early 1980s (Figure 12, right, signals mostly confined between 2- and 4-year cycles), although such relationship was not as strong as on the other coasts.

Spectral analyses for the SAM, ZW3, PDO, and IOD were also performed (not shown), and their most noteworthy results are described as follows. The most

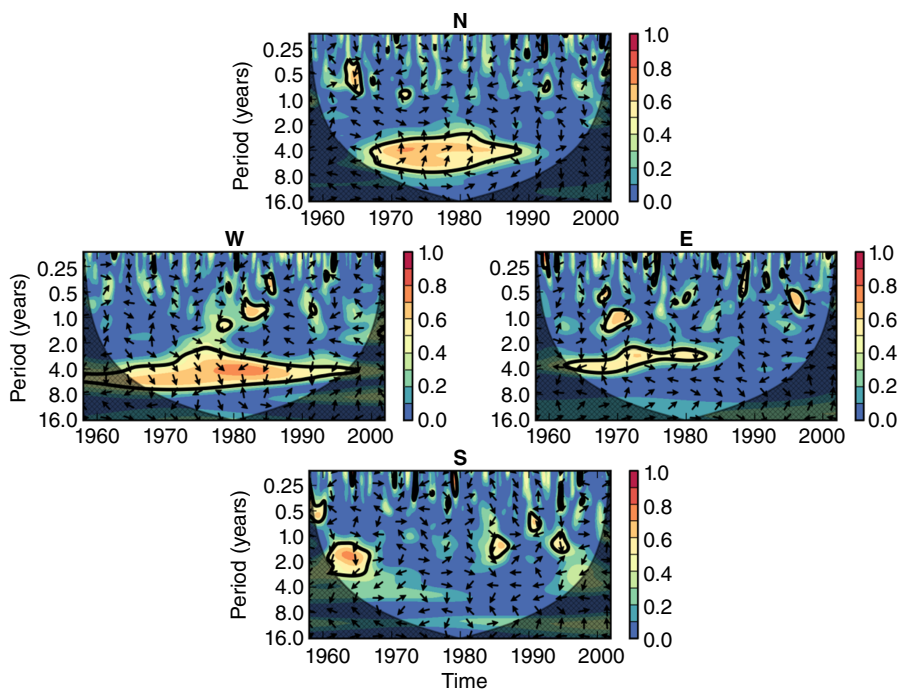


Figure 12. Squared wavelet coherence spectra of monthly anomalies of the storm cluster indices with monthly anomalies of the SOI. Thick contours represent 90% confidence levels, while hatched areas represent the cone-of-influence. In phase and antiphase signals are represented by arrows pointing upwards and downwards, respectively. Arrows pointing rightwards represent the ENSO preceding SWCs, whereas the converse is true for arrows pointing leftwards. The letters N, W, E, and S on top of each plot stand for north, west, east, and south coasts, respectively.

striking feature of the coherence spectra obtained for the SAM appeared at timescales between 6 and 16 years, and resulted in a higher occurrence of clustered storms to the south of New Zealand during its positive phase. A large part of this signal is within the cone-of-influence, a region of the spectrum where edge effects become important (Torrence and Compo, 1998), requiring caution in the interpretation of the results. Despite that, considerably high statistically significant correlations (up to 0.9) were found at those timescales during the whole period of analysis, with the strongest signals appearing first in the early 1990s. This strengthening in the correlation on the south coast throughout the time seems to accompany the trend for a positive SAM. On the west coast, a prolonged negative SAM (Gordon *et al.*, 2007) was strongly correlated (up to 0.8) with increases in clustered storms from the late 1960s to the early 1970s, supporting the negative monthly and seasonal linear correlations discussed previously. Similarly to the spectra for the SAM, the coherence spectra of the ZW3 Index with storm cluster indices showed strong correlations (up to 0.8) in the south at timescales longer than 6 years. These correlations appeared in approximately 1987, indicating that increases in clustered storms coincided with positive anomalies in the northwards atmospheric flow. Again, although within the cone-of-influence, such correlations were statistically significant. The migration from a more zonal to a more meridional atmospheric flow (a transition to the ZW3 positive phase) in 1997 (Raphael, 2004) was highly correlated (correlation >0.9) with a brief decrease in clustering on the west coast. The opposite atmospheric change

(from meridional to zonal flow) in 1986/1987 (Raphael, 2004) led to more clustered storms on the same coast. A 2-year PDO cycle was associated with a strange and counter-intuitive clustering (fewer clustered storms, correlation >0.6) to the south of New Zealand throughout the 1980s, when the PDO was predominantly positive (Mantua *et al.*, 1997). On the east coast, the same happened for the PDO decadal variability from the late 1980s to the early 2000s (signal within the cone-of-influence), while cycles ranging from 2 to 8 years were related to more clustering from the late 1950s to the early 1970s (correlation >0.7, signal partially within the cone-of-influence). The positive IOD was strongly correlated (correlation up to 0.9) with clustering on the west coast from the mid-1970s to the early 2000s. Since the mid-1980s, clustering on the west coast under El Niño-like conditions seemed more associated with a positive IOD than a negative ENSO. Two extreme positive IOD events occurred in 1994 and 1997 (Saji *et al.*, 1999) and were related to more clustered storms on the west coast owing to the intensification of southwesterly winds. From the early 1980s to the early 1990s, decreases in clustering on the north coast occurred during positive IOD, whereas stronger northeasterly winds (La Niña-like conditions associated with negative IOD) induced more clustered storms.

3. Conclusions

Work on coastal erosion has shown that storms are more hazardous when occurring in clusters because the coastline

has insufficient time to recover between storms (Lee *et al.*, 1998; Ferreira, 2005). The reserves of sand in the beach-face deplete during the first storm, facilitating erosion during subsequent ones. Here, SWCs and their characteristics in New Zealand waters were explored using results of a 45-year (1957–2002) wave hindcast. Cluster duration, the number of storms within the cluster, and the potential for cluster-induced coastal erosion were analysed through long-term averages and trends. The responses of clustered storms to near and remote atmospheric variability were also addressed, by computing correlation coefficients and applying the wavelet spectral analysis.

Storm waves tended to cluster more to the northeast of New Zealand and on the central eastern coast of the South Island. Recurrent southwesterly swells, generated by extratropical cyclones, produced energetic environments to the south of New Zealand and on the northwestern coast, making these regions the most vulnerable to coastal erosion caused by SWCs. SWCs lasted longest on a segment of the east coast of the South Island sheltered from the prevailing southwesterly swell, where they were also least frequent. Trends calculated for the period 1958–2001 showed that SWCs have incorporated more storms, have become more hazardous, and have lasted longer, principally around the South Island. Although these trends may be affected by the ERA-40 data assimilation temporal inhomogeneity, it is encouraging that they agree with trends in the SAM, PDO, and ENSO.

Teleconnection patterns showed strong links with storm wave clustering around New Zealand. These links arise in several forms, as for example, ENSO-related effects are experienced in the area because of the pressure seesaw between the Indian and Pacific Oceans (Kousky *et al.*, 1984); the extratropical signature of the ENSO projects onto the SAM (L'Heureux and Thompson, 2006) in the wave generation zone of the primary swell that hits New Zealand; variations associated with the IOD are explained by Rossby wave trains, which propagate from the tropical Indian Ocean and induce changes to the mid-latitude westerlies across southern Australia (Cai *et al.*, 2011). As a result of remote and local forcings, seasonal to decadal variabilities of climate patterns were found to be correlated with clustering around New Zealand, especially during strong phases of the modes. Stronger southwesterly winds during either El Niño events (negative ENSO) or conditions that resemble these, associated with positive phases of the IOD and PDO, caused increases in clustering primarily on the southwestern coast of New Zealand. The opposite phases of these oscillations, especially positive ENSO and negative IOD, affected the north coast through the predominance of increased northeasterly winds. Clustered storms were less synchronized with the ENSO, IOD, and PDO, whose main signatures take place far away from New Zealand, than with the SAM and ZW3 modes, which in turn show their main signatures in the water bodies surrounding the country. The strong eastwards atmospheric zonal flow related to negative ZW3 led to a higher occurrence of clustered storms on the west coast, while enhanced westerlies associated with positive SAM had

a significant impact on clustering to the south of New Zealand.

As an emerging topic, the spatial and temporal variabilities of storm wave clustering still need further research along most coasts around the world. Because of the strong influence of SWCs on erosion processes, sediment transport, and coastal flooding, a broad understanding of the dynamics of SWCs should underpin coastal management. Moreover, as undoubtedly dangerous systems, SWCs have a direct impact on safety and, consequently, on the economy. It is still not clear how storm wave clustering changes with the seasons and with anomalies associated with concurrent phases of two or more atmospheric oscillations. Additionally, our study focused on the potential effect of clustering on erosion, but has not addressed how this translates into the scale of erosion on a particular beach. The study of the latter necessitates a much wider range of local observations to provide a similarly generalizable outcome. Nevertheless, the results presented here should assist in the prediction of impacts of future climate change in addition to supporting sea-related activities and providing a background for climatological studies.

Acknowledgements

This research was funded by CAPES (grant no. BEX9551/13-1), New Zealand Ministry of Science and Innovation (contract C01X0806), and Hazards Platform (contract C05X0907). We are thankful to Marilyn Raphael, NOAA, ECMWF, JAMSTEC, BAS, and JMA for data provision, and to the reviewers for insightful comments that led to improvements in the article.

References

- Almeida LP, Voudoukas MV, Ferreira Ó, Rodrigues BA, Matias A. 2012. Thresholds for storm impacts on an exposed sandy coastal area in southern Portugal. *Geomorphology* **143–144**: 3–12. <https://doi.org/10.1016/j.geomorph.2011.04.047>.
- Alves JHGM, Young IR. 2003. On estimating extreme wave heights using combined Geosat, Topex/Poseidon and ERS-1 altimeter data. *Appl. Ocean Res.* **25**: 167–186. <https://doi.org/10.1016/j.apor.2004.01.002>.
- Arblaster JM, Meehl GA. 2006. Contributions of external forcings to Southern Annular Mode trends. *J. Clim.* **19**: 2896–2905. <https://doi.org/10.1175/JCLI3774.1>.
- Balouin Y, Tesson J, Gervais M. 2013. Cuspate shoreline relationship with nearshore bar dynamics during storm events – field observations at Sète beach, France. *J. Coastal Res.* **1**: 440–445. <https://doi.org/10.2112/SI65-075.1>.
- Benavente J, Del Río L, Plomaritis TA, Menapace W. 2013. Impact of coastal storm in a sandy barrier (Sancti Petri, Spain). *J. Coastal Res.* **1**: 666–671. <https://doi.org/10.2112/SI65-113.1>.
- Birkemeier WA, Nicholls RJ, Lee G. 1999. Storms, storm groups and nearshore morphologic change. In *Coastal Sediments '99, International symposium; 4th, Coastal engineering and science of coastal sediment processes*, Vol. **1–3**, Kraus NC, McDougal W (eds). ASCE: Hauppauge, NY, 1109–1122.
- Bjerknes J. 1966. A possible response of the atmospheric Hadley circulation to equatorial anomalies of ocean temperature. *Tellus A* **18**(4): 820–829. <https://doi.org/10.1111/j.2153-3490.1966.tb00303.x>.
- Bromwich DH, Fogt RL. 2004. Strong trends in the skill of the ERA-40 and NCEP–NCAR reanalyses in the high and midlatitudes of the Southern Hemisphere, 1958–2001. *J. Clim.* **17**: 4603–4619. <https://doi.org/10.1175/3241.1>.

- Cai W, Baines PG, Gordon HB. 1999. Southern mid- to high-latitude variability, a zonal wavenumber-3 pattern, and the Antarctic circumpolar wave in the CSIRO coupled model. *J. Clim.* **12**: 3087–3104. [https://doi.org/10.1175/1520-0442\(1999\)012<3087:SMTHLV>2.0.CO;2](https://doi.org/10.1175/1520-0442(1999)012<3087:SMTHLV>2.0.CO;2).
- Cai W, van Rensch P, Cowan T. 2011. Teleconnection pathways of ENSO and the IOD and the mechanisms for impacts on Australian rainfall. *J. Clim.* **24**: 3910–3923. <https://doi.org/10.1175/2011JCLI4129.1>.
- Cai W, Borlace S, Lengaigne M, van Rensch P, Collins M, Vecchi G, Timmermann A, Santoso A, McPhaden MJ, Wu L, England MH, Wang G, Guilyardi E, Jin F-F. 2014. Increasing frequency of extreme El Niño events due to greenhouse warming. *Nat. Clim. Change* **4**: 111–116. <https://doi.org/10.1038/nclimate2100>.
- Cai W, Wang G, Santoso A, McPhaden MJ, Wu L, Jin F, Timmermann A, Collins M, Vecchi G, Lengaigne M, England MH, Dommegiet D, Takahashi K, Guilyardi E. 2015. Increased frequency of extreme La Niña events under greenhouse warming. *Nat. Clim. Change* **5**: 132–137. <https://doi.org/10.1038/nclimate2492>.
- Coco G, Senechal N, Rejas A, Bryan KR, Capo S, Parisot JP, Brown JA, MacMahan JHM. 2014. Beach response to a sequence of extreme storms. *Geomorphology* **204**: 493–501. <https://doi.org/10.1016/j.geomorph.2013.08.028>.
- Deser C, Alexander MA, Xie S, Phillips AS. 2010. Sea surface temperature variability: patterns and mechanisms. *Annu. Rev. Mar. Sci.* **2**: 115–143. <https://doi.org/10.1146/annurev-marine-120408-151453>.
- Dissanayake P, Brown J, Karunarathna H. 2015a. Impacts of storm chronology on the morphological changes of the Formby beach and dune system, UK. *Nat. Hazards Earth Syst. Sci.* **15**: 1533–1543. <https://doi.org/10.5194/nhess-15-1533-2015>.
- Dissanayake P, Brown J, Wisse P, Karunarathna H. 2015b. Comparison of storm cluster vs isolated event impacts on beach/dune morphodynamics. *Estuarine Coastal Shelf Sci.* **164**: 301–312. <https://doi.org/10.1016/j.ecss.2015.07.040>.
- Dissanayake P, Brown J, Wisse P, Karunarathna H. 2015c. Effects of storm clustering on beach/dune evolution. *Mar. Geol.* **370**: 63–75. <https://doi.org/10.1016/j.margeo.2015.10.010>.
- Dolan R, Davis R. 1994. Coastal storm hazards. *J. Coastal Res.* **SI12**: 103–114.
- Economou T, Stephenson DB, Pinto JG, Shaffrey LC, Zappa G. 2015. Serial clustering of extratropical cyclones in a multi-model ensemble of historical and future simulations. *Q. J. R. Meteorol. Soc.* **141**(693): 3076–3087. <https://doi.org/10.1002/qj.2591>.
- Fawcett L, Walshaw D. 2008. Bayesian inference for clustered extremes. *Extremes* **11**: 217–233. <https://doi.org/10.1007/s10687-007-0054-y>.
- Ferreira Ó. 2002. Prediction of the impact of storm groups and their importance in coastal evolution. In *Proceedings of the International Conference on Coastal Engineering '02*, 7–12 July 2002, ASCE: Cardiff, Wales, UK, 2725–2730. <https://doi.org/10.1680/scc.42377.0152>.
- Ferreira Ó. 2005. Storm groups versus extreme single storms: predicted erosion and management consequences. *J. Coastal Res.* **SI42**: 221–227.
- Ferreira Ó. 2006. The role of storm groups in the erosion of sandy coasts. *Earth Surf. Processes Landforms* **31**: 1058–1060. <https://doi.org/10.1002/esp.1378>.
- Gillet NP, Thompson DWJ. 2003. Simulation of recent Southern Hemisphere climate change. *Science* **302**(5643): 273–275. <https://doi.org/10.1126/science.1087440>.
- Godoi VA, Bryan KR, Gorman RM. 2016. Regional influence of climate patterns on the wave climate of the southwestern Pacific: the New Zealand region. *J. Geophys. Res. Oceans* **121**(6): 4056–4076. <https://doi.org/10.1002/2015JC011572>.
- Godoi VA, Bryan KR, Stephens SA, Gorman RM. 2017. Extreme waves in New Zealand waters. *Ocean Modell.* **117C**: 97–110. <https://doi.org/10.1016/j.ocemod.2017.08.004>.
- Gordon ND. 1986. The Southern Oscillation and New Zealand weather. *Mon. Weather Rev.* **14**: 371–387. [https://doi.org/10.1175/1520-0493\(1986\)114<371:TSOANZ>2.0.CO;2](https://doi.org/10.1175/1520-0493(1986)114<371:TSOANZ>2.0.CO;2).
- Gordon AL, Visbeck M, Comiso JC. 2007. A possible link between the Weddell Polynya and the Southern Annular Mode. *J. Clim.* **20**: 2558–2571. <https://doi.org/10.1175/JCLI4046.1>.
- Gorman RM, Bryan KR, Laing AK. 2003. Wave hindcast for the New Zealand region: deep-water wave climate. *N. Z. J. Mar. Freshw. Res.* **37**(3): 589–612. <https://doi.org/10.1080/00288330.2003.9517191>.
- Gorman RM, Bell RG, Lane EM, Gillibrand PA, Stephens SA. 2010. New Zealand wave climate – simulating the past and future. In *New Zealand Coastal Society Annual Conference*, New Zealand Coastal Society, Whitianga, New Zealand, 17–19 November 2010.
- Grimm AM, Ambrizzi T. 2009. Teleconnections into South America from the Tropics and extratropics on interannual and intraseasonal timescales. Past climate variability in South America and surrounding regions. *Dev. Paleoenvir. Res.* **14**: 159–191. https://doi.org/10.1007/978-90-481-2672-9_7.
- Gupta AS, England MH. 2007. Coupled ocean–atmosphere feedback in the Southern Annular Mode. *J. Clim.* **20**: 3677–3692. <https://doi.org/10.1175/JCLI4200.1>.
- Harley MD, Turner IL, Short AD, Ranasinghe R. 2009. An empirical model of beach response to storms – SE Australia. In *Coasts and Ports 2009: In a Dynamic Environment*. Engineers Australia: Wellington, 600–606.
- Harley MD, Turner IL, Short AD, Ranasinghe R. 2010. Interannual variability and controls of the Sydney wave climate. *Int. J. Climatol.* **30**: 1322–1335. <https://doi.org/10.1002/joc.1962>.
- Hayward TL. 1993. Preliminary observations of the 1991–1992 El Niño in the California Current. California Cooperative Oceanic Fisheries Investigations Reports No. 34, California Cooperative Oceanic Fisheries Investigations: California, 21–29. http://calcofi.org/publications/calcofireports/v34/Vol_34_Status_CC_Hayward.pdf (accessed 29 November 2017).
- Hemer MA, Church JA, Hunter JR. 2010. Variability and trends in the directional wave climate of the Southern Hemisphere. *Int. J. Climatol.* **30**(4): 475–491. <https://doi.org/10.1002/joc.1900>.
- Izumo T, Vialard J, Lengaigne M, Montegut CB, Behera SK, Luo J, Cravatte S, Masson S, Yamagata T. 2010. Influence of the state of the Indian Ocean Dipole on the following year's El Niño. *Nat. Geosci.* **3**: 168–172. <https://doi.org/10.1038/ngeo760>.
- Jury MR, Enfield DB, Mélice J-L. 2002. Tropical monsoons around Africa: stability of El Niño–Southern Oscillation associations and links with continental climate. *J. Geophys. Res.* **107**(C10): 3151. <https://doi.org/10.1029/2000JC000507>.
- Karunarathna H, Pender D, Ranasinghe R, Short AD, Reeve DE. 2014. The effects of storm clustering on beach profile variability. *Mar. Geol.* **348**: 103–112. <https://doi.org/10.1016/j.margeo.2013.12.007>.
- Kendall MG. 1955. *Rank Correlation Methods*, 2nd edn. Charles Griffin and Company: London.
- Kousky VE, Kagano MT, Cavalcanti IFA. 1984. A review of the Southern Oscillation: oceanic–atmospheric circulation changes and related rainfall anomalies. *Tellus A* **36**(5): 490–504. <https://doi.org/10.1111/j.1600-0870.1984.tb00264.x>.
- Kriebel DL, Dean RG. 1993. Convolution method for time-dependent beach-profile response. *J. Waterw. Port Coastal Ocean Eng.* **119**(2): 204–226. [https://doi.org/10.1061/\(ASCE\)0733-950X\(1993\)119:2\(204\)](https://doi.org/10.1061/(ASCE)0733-950X(1993)119:2(204)).
- Kushner PJ, Held IM, Delworth TL. 2001. Southern Hemisphere atmospheric circulation response to global warming. *J. Clim.* **14**: 2238–2249. [https://doi.org/10.1175/1520-0442\(2001\)014<2238:SHACRT>2.0.CO;2](https://doi.org/10.1175/1520-0442(2001)014<2238:SHACRT>2.0.CO;2).
- Kvamstø NG, Song Y, Seierstad IA, Sorteberg A, Stephenson DB. 2008. Clustering of cyclones in the ARPEGE general circulation model. *Tellus A* **60**(3): 547–556. <https://doi.org/10.1111/j.1600-0870.2008.00307.x>.
- L'Heureux ML, Thompson DWJ. 2006. Observed relationships between the El Niño–Southern Oscillation and the extratropical zonal-mean circulation. *J. Clim.* **19**: 276–287. <https://doi.org/10.1175/JCLI3617.1>.
- Laing AK. 2000. New Zealand wave climate from satellite observations. *N. Z. J. Mar. Freshw. Res.* **34**(4): 727–744. <https://doi.org/10.1080/00288330.2000.9516973>.
- Lee G, Nicholls RJ, Birkemeier WA. 1998. Storm-driven variability of the beach-nearshore profile at Duck, North Carolina, USA, 1981–1991. *Mar. Geol.* **148**: 163–177. [https://doi.org/10.1016/S0025-3227\(98\)00010-3](https://doi.org/10.1016/S0025-3227(98)00010-3).
- Liu Z, Alexander M. 2007. Atmospheric bridge, oceanic tunnel, and global climatic teleconnections. *Rev. Geophys.* **45**: RG2005. <https://doi.org/10.1029/2005RG000172>.
- Lopatoukhin LJ, Rozhkov VA, Ryabinin VE, Swail VR, Boukhanovsky AV, Degtyarev AB. 2000. Estimation of extreme wave heights. WMO/TD-No. 1041. JCOMM Technical Report No. 9, World Meteorological Organisation, Intergovernmental Oceanographic Commission (of UNESCO): Geneva, Switzerland, 73 p.
- Loureiro C, Ferreira Ó, Cooper JAG. 2009. Contrasting morphologic behaviour at embayed beaches in southern Portugal. *J. Coastal Res.* **SI56**: 83–87.
- Loureiro C, Ferreira Ó, Cooper JAG. 2012. Extreme erosion on high-energy embayed beaches: influence of megarips and storm grouping. *Geomorphology* **139–140**: 155–171. <https://doi.org/10.1016/j.geomorph.2011.10.013>.

- Mailier PJ, Stephenson DB, Ferro CAT. 2006. Serial clustering of extratropical cyclones. *Mon. Weather Rev.* **134**: 2224–2240. <https://doi.org/10.1175/MWR3160.1>.
- Mann HB. 1945. Nonparametric tests against trend. *Econometrica* **13**(3): 245–259. <https://doi.org/10.2307/1907187>.
- Mantua NJ, Hare SR, Zhang Y, Wallace JM, Francis RC. 1997. A Pacific interdecadal climate oscillation with impacts on salmon production. *Bull. Am. Meteorol. Soc.* **78**(6): 1069–1079. [https://doi.org/10.1175/1520-0477\(1997\)078<1069:APICOW>2.0.CO;2](https://doi.org/10.1175/1520-0477(1997)078<1069:APICOW>2.0.CO;2).
- Marshall GJ. 2003. Trends in the Southern Annular Mode from observations and reanalyses. *J. Clim.* **16**(24): 4134–4143. [https://doi.org/10.1175/1520-0442\(2003\)016<4134:TITSAM>2.0.CO;2](https://doi.org/10.1175/1520-0442(2003)016<4134:TITSAM>2.0.CO;2).
- Mathiesen M, Goda Y, Hawkes PJ, Mansard E, Martin MJ, Peltier E, Thompson EF, Vledder GV. 1994. Recommended practice for extreme wave analysis. *J. Hydraul. Res.* **32**(6): 803–814. <https://doi.org/10.1080/00221689409498691>.
- McPhaden MJ, Timmermann A, Widlansky MJ, Balmaseda MA, Stockdale TN. 2015. The curious case of the El Niño that never happened: a perspective from 40 years of progress in climate research and forecasting. *Bull. Am. Meteorol. Soc.* **96**: 1647–1665. <https://doi.org/10.1175/BAMS-D-14-00089.1>.
- Méndez FJ, Menéndez M, Luceño A, Losada IJ. 2006. Estimation of the long-term variability of extreme significant wave height using a time-dependent peak over threshold (POT) model. *J. Geophys. Res.* **111**: C07024. <https://doi.org/10.1029/2005JC003344>.
- Mendoza ET, Jimenez JA. 2006. Storm-induced beach erosion potential on the Catalonian coast. *J. Coastal Res.* **SI48**: 81–88.
- Nunes M, Ferreira Ó, Loureiro C, Baily B. 2011. Beach and cliff retreat induced by storm groups at Forte Novo, Algarve (Portugal). *J. Coastal Res.* **SI64**: 795–799.
- Pezza AB, Simmonds I, Renwick JA. 2007. Southern Hemisphere cyclones and anticyclones: recent trends and links with decadal variability in the Pacific Ocean. *Int. J. Climatol.* **27**(11): 1403–1419. <https://doi.org/10.1002/joc.1477>.
- Phillips MS, Turner IL, Cox RJ, Splinter KD, Harley MD. 2015. Will the sand come back?: observations and characteristics of beach recovery. In *Australasian Coasts & Ports Conference 2015: 22nd Australasian Coastal and Ocean Engineering Conference and the 15th Australasian Port and Harbour Conference*, Engineers Australia and IPENZ, Auckland, New Zealand, 676–682. ISBN: 9781922107794.
- Pickrill RA, Mitchell JS. 1979. Ocean wave characteristics around New Zealand. *N. Z. J. Mar. Freshw. Res.* **13**(4): 501–520. <https://doi.org/10.1080/00288330.1979.9515827>.
- Pinto JG, Bellenbaum N, Karrenmann MK, Della-Marta PM. 2013. Serial clustering of extratropical cyclones over the North Atlantic and Europe under recent and future climate conditions. *J. Geophys. Res. Atmos.* **118**(22): 12476–12485. <https://doi.org/10.1002/2013JD020564>.
- Pinto JG, Gómez I, Masato G, Dacre HF, Woollings T, Caballero R. 2014. Large-scale dynamics associated with clustering of extratropical cyclones affecting western Europe. *J. Geophys. Res. Atmos.* **119**: 13704–13719. <https://doi.org/10.1002/2014JD022305>.
- Raphael MN. 2004. A zonal wave 3 index for the Southern Hemisphere. *Geophys. Res. Lett.* **31**: L23212. <https://doi.org/10.1029/2004GL020365>.
- Saji NH, Goswami BN, Vinayachandran PN, Yamagata T. 1999. A dipole mode in the tropical Indian Ocean. *Nature* **401**: 360–363. <https://doi.org/10.1038/43854>.
- Schott FA, Xie S, McCreary JP. 2009. Indian Ocean circulation and climate variability. *Rev. Geophys.* **47**: RG1002. <https://doi.org/10.1029/2007RG000245>.
- Sen PK. 1968. Estimates of the regression coefficient based on Kendall's tau. *J. Am. Stat. Assoc.* **63**(324): 1379–1389. <https://doi.org/10.1080/01621459.1968.10480934>.
- Senechal N, Castelle B, Bryan KR. 2017. Storm clustering and beach response. In *Coastal Storms: Processes and Impacts*. Wiley-Blackwell: New York, NY.
- Simmonds I, Keay K. 2000. Variability of Southern Hemisphere extratropical cyclone behavior, 1958–97. *J. Clim.* **13**(2): 550–561. [https://doi.org/10.1175/1520-0442\(2000\)013<0550:VOSHEC>2.0.CO;2](https://doi.org/10.1175/1520-0442(2000)013<0550:VOSHEC>2.0.CO;2).
- Sinclair MR. 1995. A climatology of cyclogenesis for the Southern Hemisphere. *Mon. Weather Rev.* **123**(6): 1601–1619. [https://doi.org/10.1175/1520-0493\(1995\)123<1601:ACOCFT>2.0.CO;2](https://doi.org/10.1175/1520-0493(1995)123<1601:ACOCFT>2.0.CO;2).
- Splinter KD, Carley JT, Golshani A, Tomlinson R. 2014. A relationship to describe the cumulative impact of storm clusters on beach erosion. *Coastal Eng.* **83**: 49–55. <https://doi.org/10.1016/j.coastaleng.2013.10.001>.
- Stephens SA, Gorman RM. 2006. Extreme wave predictions around New Zealand from hindcast data. *N. Z. J. Mar. Freshw. Res.* **40**(3): 399–411. <https://doi.org/10.1080/00288330.2006.9517431>.
- Taschetto AS, Gupta AS, Hendon HH, Ummenhofer CC, England MH. 2011. The contribution of Indian Ocean sea surface temperature anomalies on Australian summer rainfall during El Niño events. *J. Clim.* **24**: 3734–3747. <https://doi.org/10.1175/2011JCLI3885.1>.
- Theil H. 1950. A rank-invariant method of linear and polynomial regression analysis. *Proc. R. Netherlands Acad. Sci.* **53**(Part I): 386–392 (Part II): 521–525, (Part III): 1397–1412.
- Thompson DWJ, Solomon S. 2002. Interpretation of recent Southern Hemisphere climate change. *Science* **296**: 895–899. <https://doi.org/10.1126/science.1069270>.
- Tolman HL. 1991. A third-generation model for wind waves on slowly varying, unsteady, and inhomogeneous depths and currents. *J. Phys. Oceanogr.* **21**: 782–797. [https://doi.org/10.1175/1520-0485\(1991\)021<0782:ATGMFW>2.0.CO;2](https://doi.org/10.1175/1520-0485(1991)021<0782:ATGMFW>2.0.CO;2).
- Tolman HL. 2009. User manual and system documentation of WAVEWATCH III version 3.14. NOAA/NWS/NCEP/MMAB Technical Note 276, NOAA, Camp Springs, MD, 194 pp., appendices. <http://polar.ncep.noaa.gov/waves/wavewatch/wavewatch.shtml>.
- Torrence C, Compo GP. 1998. A practical guide to wavelet analysis. *Bull. Am. Meteorol. Soc.* **79**(1): 61–78. [https://doi.org/10.1175/1520-0477\(1998\)079<0061:APGTWA>2.0.CO;2](https://doi.org/10.1175/1520-0477(1998)079<0061:APGTWA>2.0.CO;2).
- Trenberth KE, Hoar TJ. 1996. The 1990–1995 El Niño–Southern Oscillation event: longest on record. *Geophys. Res. Lett.* **23**(1): 57–60. <https://doi.org/10.1029/95GL03602>.
- Uppala SM, Kallberg PW, Simmons AJ, Andrae U, Bechtold VDC, Fiorino M, Gibson JK, Haseler J, Hernandez A, Kelly GA, Li X, Onogi K, Saarinen S, Sokka N, Allan RP, Andersson E, Arpe K, Balmaseda MA, Beljaars ACM, Berg LVD, Bidlot J, Bormann N, Caires S, Chevallier F, Dethof A, Dragosavac M, Fisher M, Fuente M, Hagemann S, Hólm E, Hoskins BJ, Isaksen L, Janssen PAEM, Jenne R, McNally AP, Mahfouf J-F, Morcrette J-J, Rayner NA, Saunders RW, Simon P, Sterl A, Trenberth KE, Untch A, Vasiljevic D, Viterbo P, Woollen J. 2005. The ERA-40 re-analysis. *Q. J. R. Meteorol. Soc.* **131**(612): 2961–3012. <https://doi.org/10.1256/qj.04.176>.
- Villarini G, Smith JA, Vitolo R, Stephenson DB. 2013. On the temporal clustering of US floods and its relationship to climate teleconnection patterns. *Int. J. Climatol.* **33**(3): 629–640. <https://doi.org/10.1002/joc.3458>.
- Vitolo R, Stephenson DB, Cook IM, Mitchell-Wallace K. 2009. Serial clustering of intense European storms. *Meteorol. Z.* **18**(4): 411–424. <https://doi.org/10.1127/0941-2948/2009/0393>.
- Vousdoukas MI, Almeida LP, Ferreira Ó. 2011. Modelling storm-induced beach morphological change in a meso-tidal, reflective beach using XBeach. *J. Coastal Res.* **SI64**: 1916–1920.
- Wang G, Cai W. 2013. Climate-change impact on the 20th-century relationship between the Southern Annular Mode and global mean temperature. *Sci. Rep.* **3**: 1–6. <https://doi.org/10.1038/srep02039>.
- World Bank Group. 2016. *Global Economic Prospects, January 2016: Spillovers Amid Weak Growth*. World Bank: Washington, DC. <https://doi.org/10.1596/978-1-4648-0675-9>.
- Wyrtki K. 1975. El Niño – the dynamic response of the equatorial Pacific Ocean to atmospheric forcing. *J. Phys. Oceanogr.* **5**: 572–584. [https://doi.org/10.1175/1520-0485\(1975\)005<0572:ENTDRO>2.0.CO;2](https://doi.org/10.1175/1520-0485(1975)005<0572:ENTDRO>2.0.CO;2).
- Young IR, Zieger S, Babanin AV. 2011. Global trends in wind speed and wave height. *Science* **332**: 451–455. <https://doi.org/10.1126/science.1197219>.